Supplementary Information for

Flame-Retardant Porous Hexagonal Boron Nitride for Safe and Effective Radioactive Iodine Capture

Juan Wang [ab], Kelong Ai*[ab] and Lehui Lu *[ab]

[a] State Key Laboratory of Electroanalytical Chemistry, Changchun Institute of Applied Chemistry, Chinese Academy of Sciences, Changchun, Jilin, 130022, China.

[b] University of Science and Technology of China, Hefei, Anhui, 230026, China.

***Corresponding Author**
E-mail: klai@ciac.ac.cn; lehuilu@ciac.ac.cn.

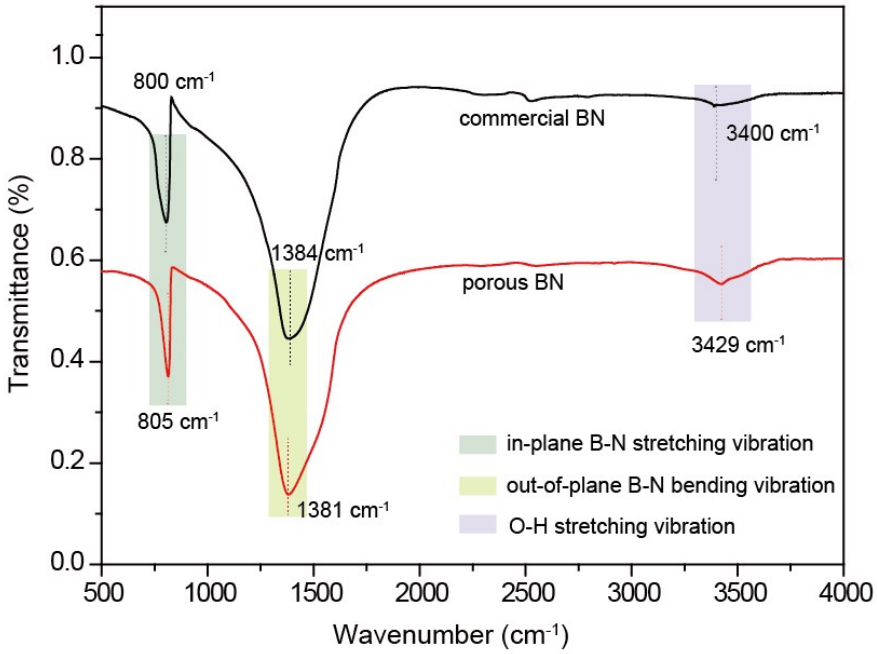

Figure S1. The FTIR spectra of the porous BN and the commercial BN materials.

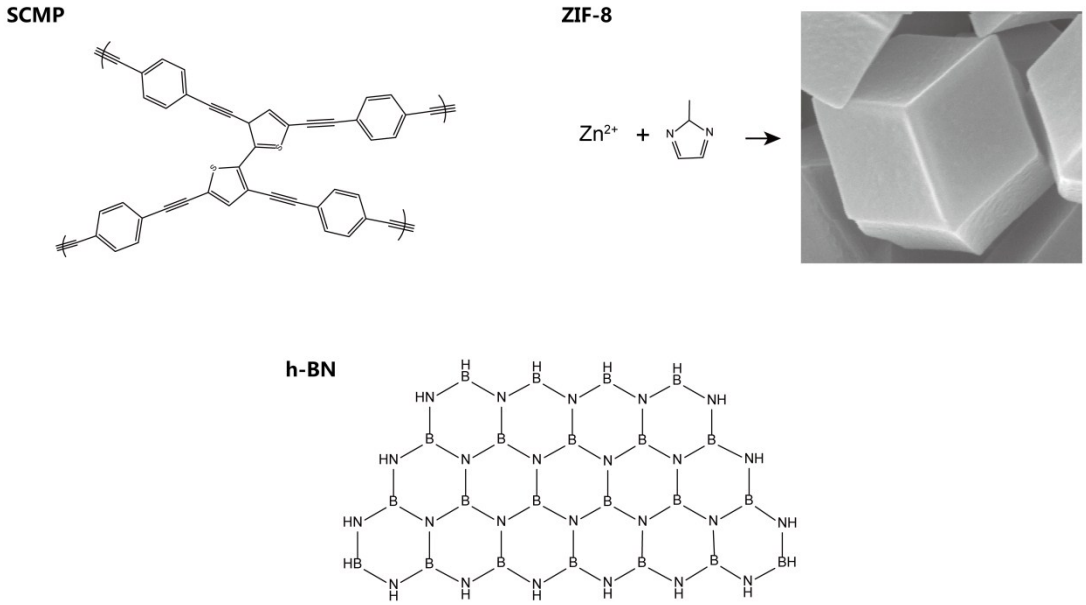

Figure S2. The networking structure of the SCMP, ZIF-8 and h-BN materials.

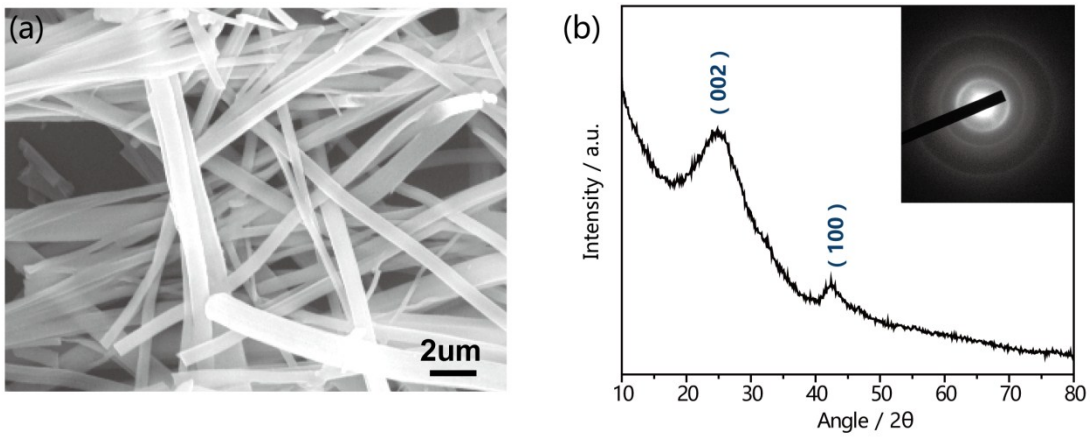

Figure S3. (a) SEM of porous BN after exposed to the elevated temperature; (b) corresponding XRD image of porous BN after exposed. Insert: the electron diffraction pattern.

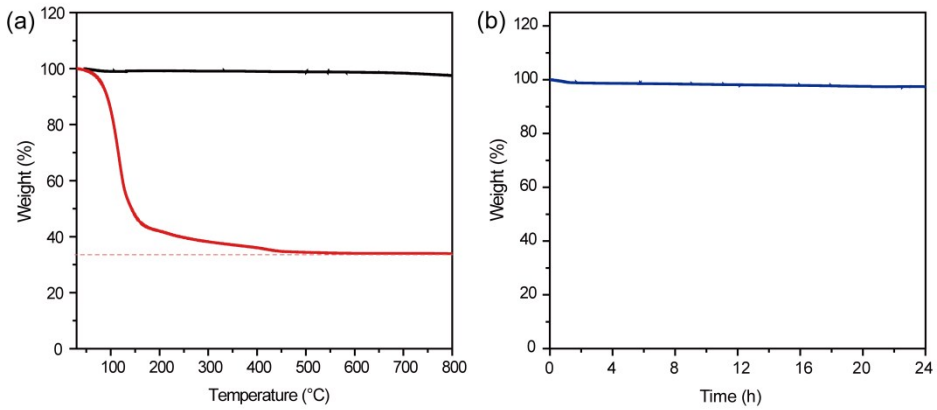

Figure S4. (a) The TGA at N_2 atmosphere of pristine porous BN (black) and the iodine–laden porous BN (red); (b) The isothermal TG profile of pristine porous BN at 125 ℃ for 24 h.

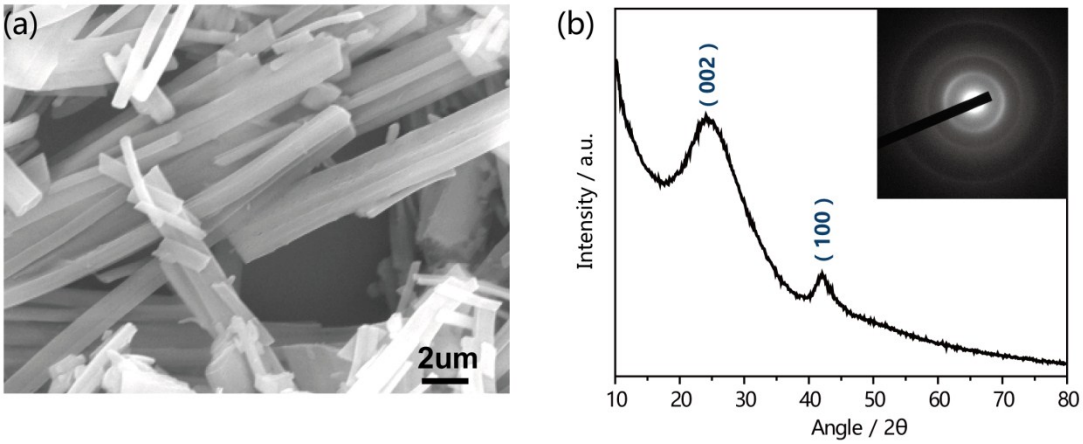

Figure S5. (a) SEM of porous BN after immersed in 5M HNO_3; (b) corresponding XRD image of porous BN after immersed. Insert: the electron diffraction pattern.

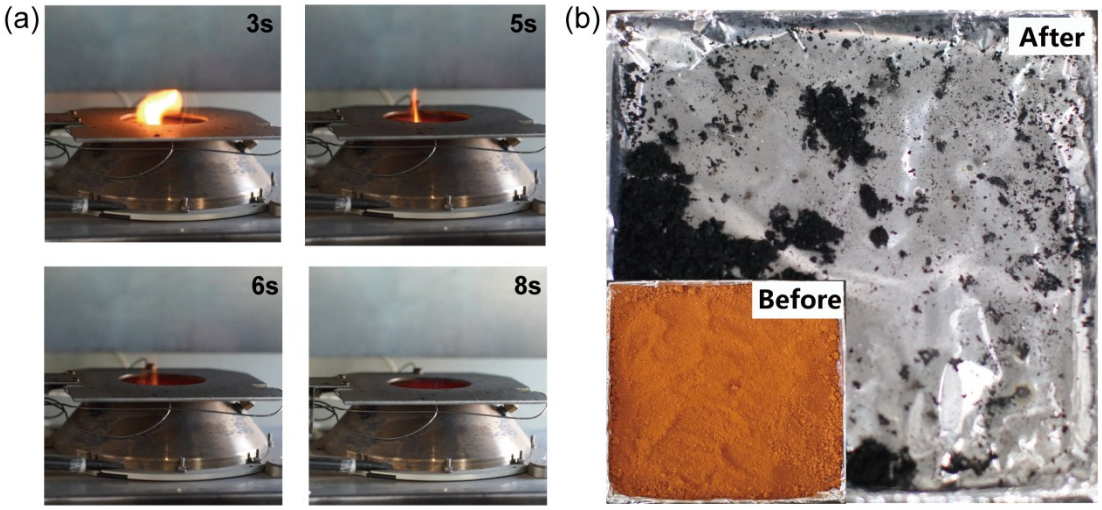

Figure S6. (a) The combustion process of the SCMP materials; (b) Residues after burning. Insets: the corresponding samples before test.

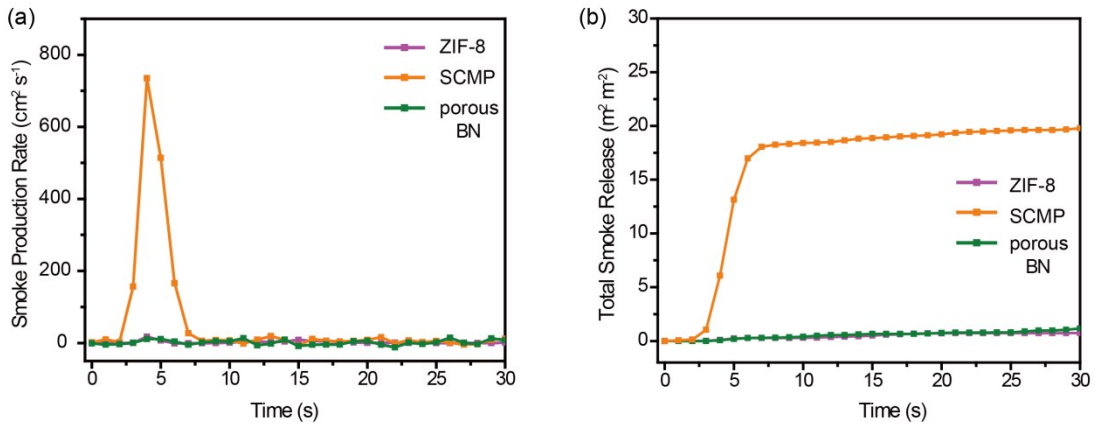

Figure S7. (a) The smoke release rate (SRR) and (b) the total smoke release (TSR) of the SCMP ZIF-8 and porous BN, respectively.

Table S1. Table for the iodine removal performance of various reported inorganic adsorbents.

Adsorbents	Iodine capacity	Temperature and pressure	S_{BET} (m^2g^{-1})	Reference
Porous BN	2.13 g/g	398K; 1bar	1043	This work
SnS	>99%[a]	398K; 1bar	456	[1]
MoSx	1.00 g/g	333K; 1bar	370	[2]
S_4-LDH	1.52 g/g	350 K; 1bar	9	[3]
HISL	0.53 g/g	298 K; 1bar	-	[4]
Cg-5P	0.87 g/g	413 K; 1bar	287	[5]
CoMoS	2.00 g/g	333 K; 1bar	360	[6]
Ag-S	75 mg/g	423 K; 15pa	109	[7]
Ag/Al_2O_3	806.9 DF Value	450 K; 1bar	107	[8]
MgO	196 mg/g	298 K; 1bar	83	[9]
SBA-15	540 mg/g	473 K; 1bar	368	[10]
C@ETS-10	40 mg/g	293 K; 1bar	149	[11]

a: capture efficiency for I_2(g).

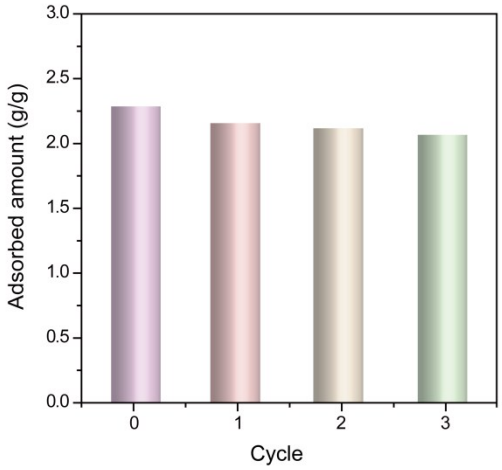

Figure S8. The adsorption experiment and cycle performance test of porous BN at 473K.

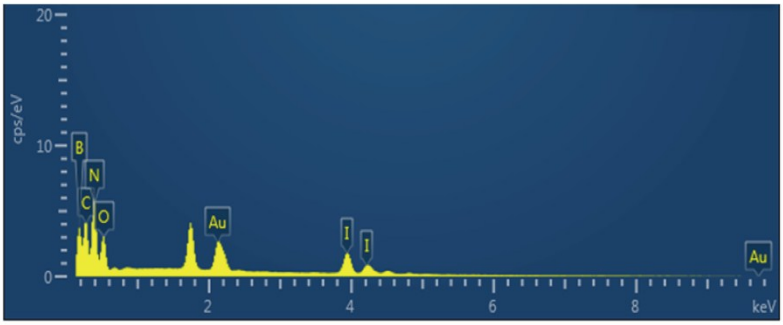

Figure S9. The EDS of porous BN after iodine loading.

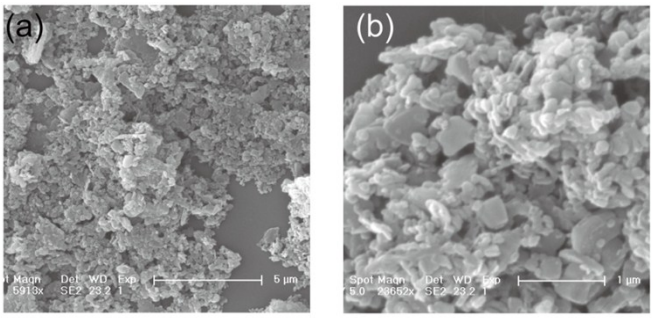

Figure S10. SEM images of cnp-BN power at different magnifications.

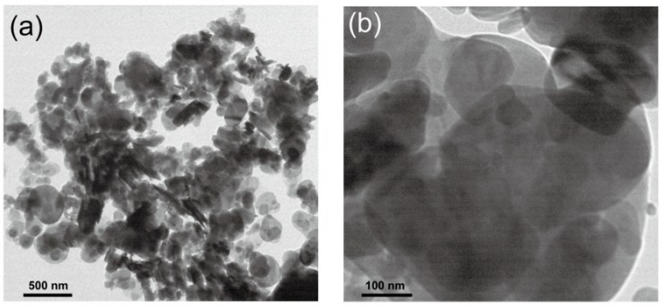

Figure S11. (a)TEM image and (b) the corresponding HRTEM image of cnp-BN power.

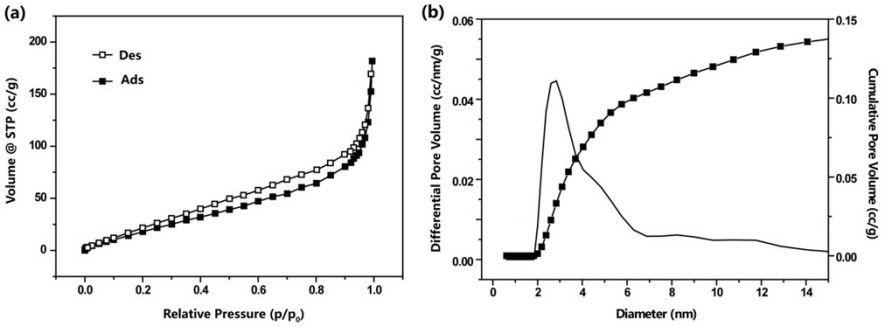

Figure S12. (a) N_2 adsorption–desorption plot at 77 K for the cnp-BN; **(b)** the corresponding pore size distributions and cumulative pore size distribution.

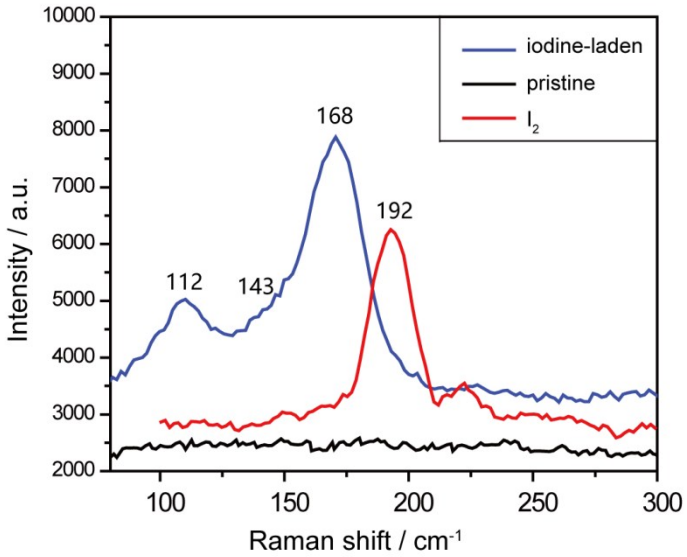

Figure S13. Raman spectra of pristine porous BN and iodine-laden porous BN.

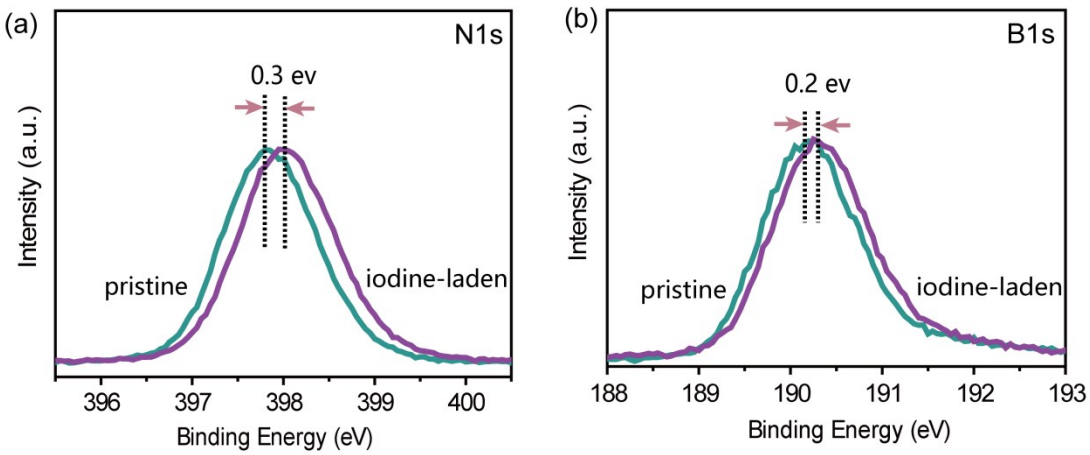

Figure S14. XPS spectra of (a) N1s and (b) B1s of the pristine porous BN and iodine-laden porous BN.

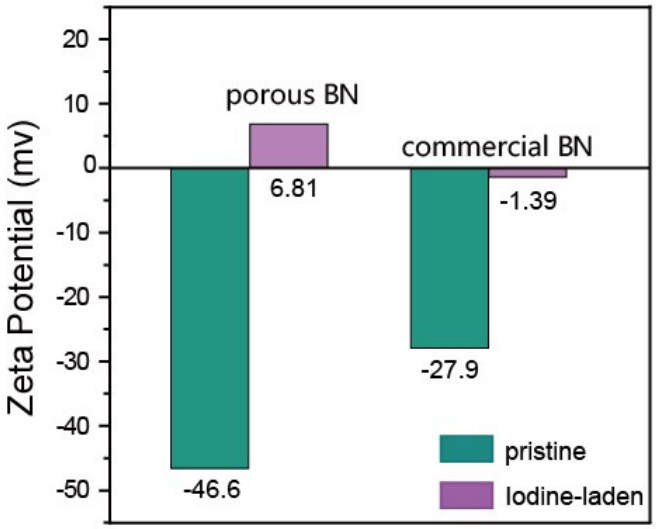

Figure S15. The Zeta potentials of porous BN and commercial-BN before and after iodine loading.

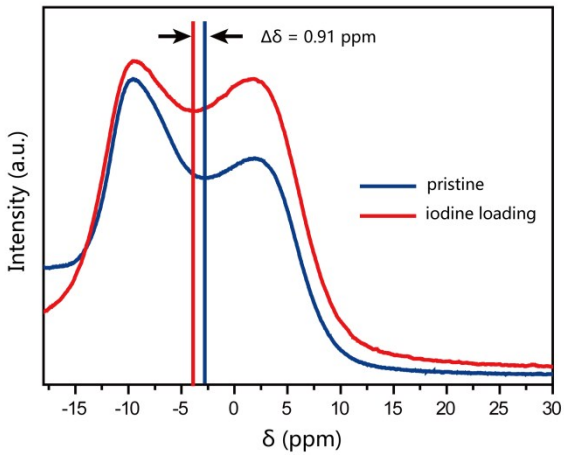

Figure S16. The ^{11}B-ssNMR of porous-BN before and after iodine loading.

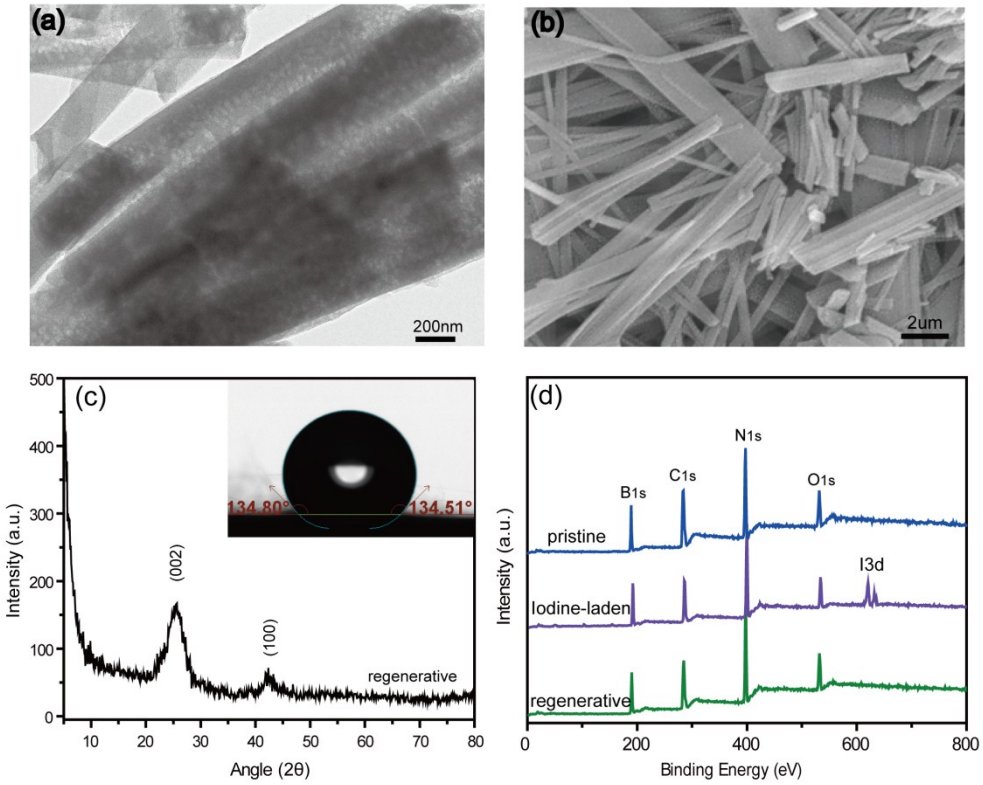

Figure S17. Characterization of regenerative porous BN: (a) TEM image; (b) SEM image; (c) the XRD profiles of the pristine and the iodine-laden porous BN; (d) XPS spectra of pristine, iodine-laden, and regenerative porous BN.

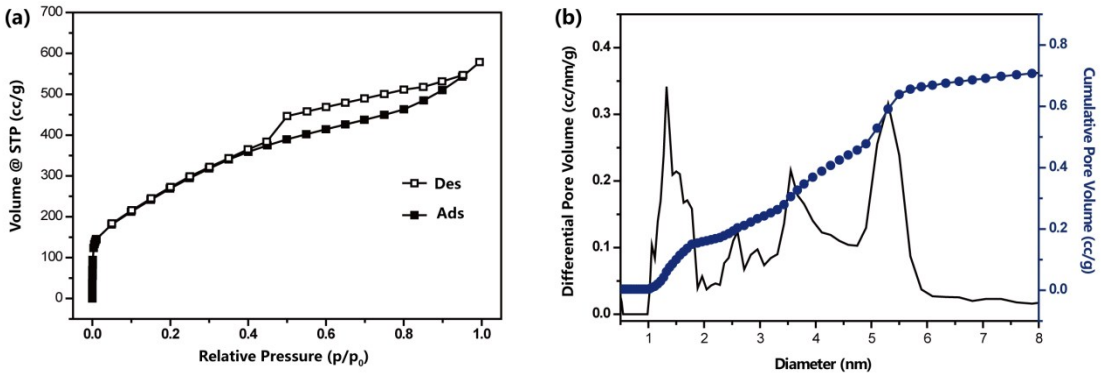

Figure S18. (a) The N_2 adsorption–desorption plot at 77 K for the regenerative porous BN and (b) the corresponding pore size distributions and cumulative pore size distribution.

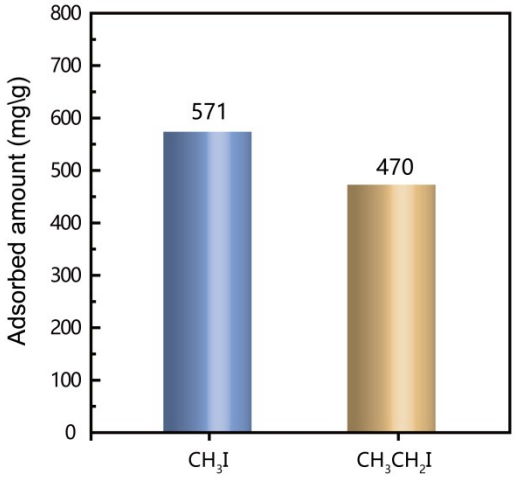

Figure S19. The adsorption capacity of porous BN on CH_3I and CH_3CH_2I (571 and 470 mg/g, respectively).

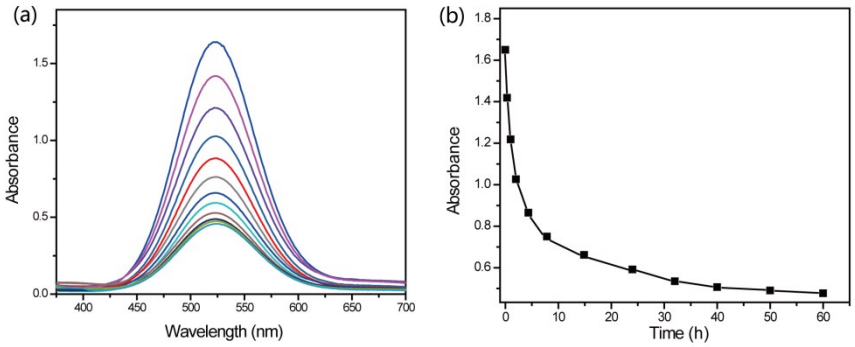

Figure S20. (a) The temporal evolution UV/vis spectra for the adsorption of I_2 in cyclohexane. (b) Kinetics curve of porous BN versus contact time in cyclohexane.

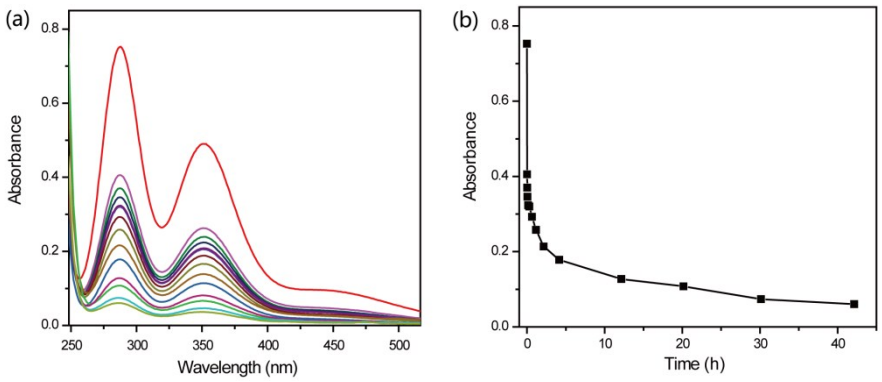

Figure S21. (a) The temporal evolution UV/vis spectra for the adsorption of iodine in aqueous solution (1% Lugol (I_2−KI) solution). (b) Kinetics curve of porous BN versus contact time in aqueous solution

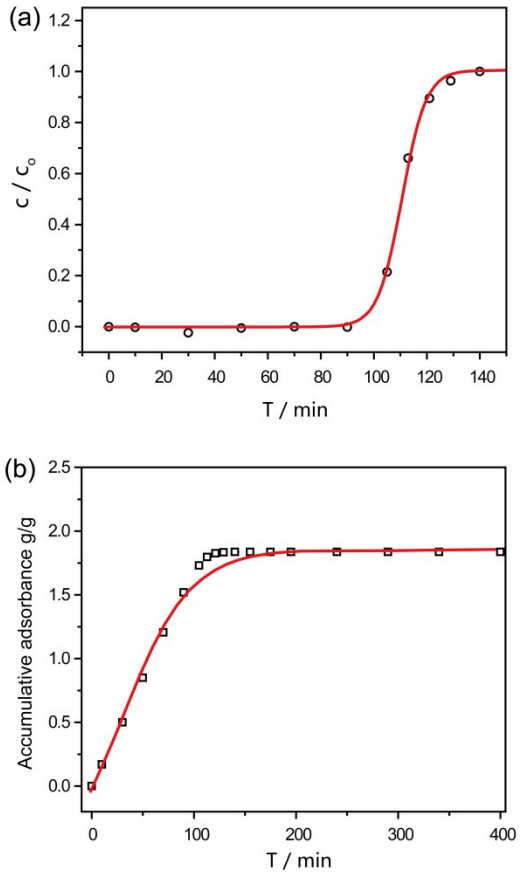

Figure S22. (a) The breakthrough curve and (b) the accumulative adsorbance of iodine for porous BN under the simulated spent nuclear fuel reprocessing conditions. It should be mentioned that the accumulative adsorbance obtained from the breakthrough experiments are slightly different from those from adsorption capacity measurements. This discrepancy is mainly due to small errors associated with factors such as the constancy of deviser, and packing density and physical adsorption of other substances.

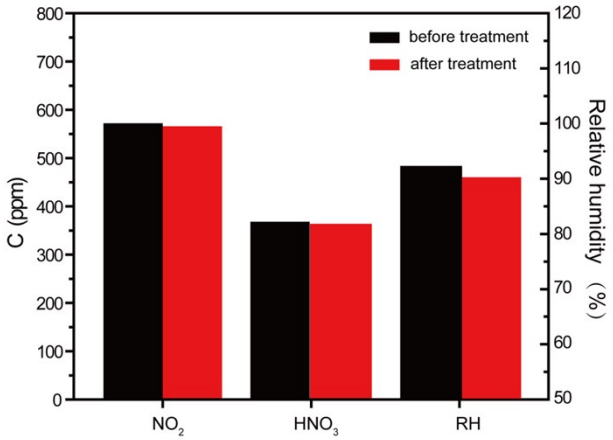

Figure S23. The concentration of NO_2 and nitric acid vapor, as well as relative humidity before and after porous BN treatment.

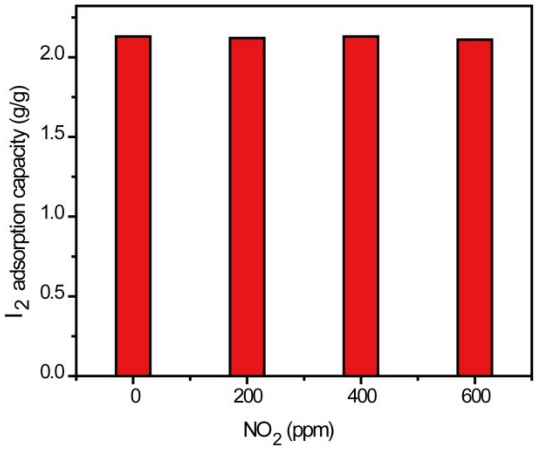

Figure S24. The amounts of iodine adsorbed by porous boron nitride at different concentration of NO_2.

Synthesis of benchmark materials:

Synthesis of ZIF-8[12]. Methanolic solutions of zinc nitrate (25 mM, 15 ml) and 2-methylimidazole (25 mM, 15 ml) were mixed and allowed to react at room temperature for 24 h without stirring. The product was collected by centrifugation, washed several times with methanol, and vacuum-dried overnight at room temperature.

Synthesis of SCMP. The SCMP was synthesized according to the literature[13]. 3,3',5,5'-tetrabromo-2,2'-bithiophene (481.8 mg, 1 mmol) and 1,4-diethynylbenzene (189.2 mg, 1.5 mmol), tetrakis (triphenylphosphine) palladium (0) (90 mg), and copper (I) iodide (30 mg) were mixed and filled with nitrogen for 20 min. After that, a mixture of toluene (5 mL) and triethylamine (5 mL) were added. Then the mixture was heated to 65 °C and stirred for 24 h under nitrogen atmosphere. The mixture was filtered and washed with methylene dichloride, acetone, water and methanol for several times. Finally, the polymer was dried overnight at 80 °C.

Reference:

1 B. J. Riley, J. Chun, W. Um, W. C. Lepry, J. Matyas, M. J. Olszta, X. Li, K. Polychronopoulou and M. G. Kanatzidis, *Environ. Sci. Technol.*, 2013, **47**, 7540-7547.

2 K. S. Subrahmanyam, C. D. Malliakas, D. Sarma, G. S. Armatas, J. Wu and M. G. Kanatzidis, *J. Am. Chem. Soc.*, 2015, **137**, 13943-13948.

3 S. L. Ma, S. M. Islam, Y. Shim, Q. Y. Gu, P. L. Wang, H. Li, G. B. Sun, X. J. Yang and M. G. Kanatzidis, *Chem. Mater.*, 2014, **26**, 7114-7123.

4 T. C. T. Pham, S. Docao, I. C. Hwang, M. K. Song, D. Y. Choi, D. Moon, P. Oleynikov and K. B. Yoon, *Energy Environ. Sci.*, 2016, **9**, 1050-1062.

5 B. J. Riley, J. Chun, J. V. Ryan, J. Matyáš, X. S. Li, D. W. Matson, S. K. Sundaram, D. M. Strachan and J. D. Vienna, *RSC. Adv.*, 2011, **1**, 1704.

6 K. S. Subrahmanyam, D. Sarma, C. D. Malliakas, K. Polychronopoulou, B. J. Riley, D. A. Pierce, J. Chun and M. G. Kanatzidis, *Chem. Mater.*, 2015, **27**, 2619-2626.

7 T. Sakurai, A. Takahashi, Y. E. Ming-lu, T. Kihara and S. Fujine, *J. Nucl. Sci. Technol.*, 1997, **34**, 211-216.

8 C. Qing-Hui, L. Ze-Jun and C. Tai-Wei, *J. Nucl. Sci. Technol.*, 2015, **26**, 040303.

9 S. U. Nandanwar, J. Dantas, K. Coldsnow, M. Green, V. Utgikar, P. Sabharwall and D. E. Aston, *Adsorption*, 2016, **22**, 335-345.

10 J. H. Yang, Y.-J. Cho, J. M. Shin and M.-S. Yim, *J. Nucl. Mater.*, 2015, **465**, 556-564.

11 S. U. Nandanwar, K. Coldsnow, M. Green, V. Utgikar, P. Sabharwall and D. E. Aston, *Chem. Eng. J.*, 2016, **287**, 593-601.

12 G. Lu, S. Li, Z. Guo, O. K. Farha, B. G. Hauser, X. Qi, Y. Wang, X. Wang, S. Han, X. Liu, J. S. DuChene, H. Zhang, Q. Zhang, X. Chen, J. Ma, S. C. Loo, W. D. Wei, Y. Yang, J. T. Hupp and F. Huo, *Nat. Chem.*, 2012, **4**, 310-316.

13 F. Ren, Z. Zhu, X. Qian, W. Liang, P. Mu, H. Sun, J. Liu and A. Li, *Chem. Commun.*, 2016, **52**, 9797-9800.